Journal of Wind Engineering & Industrial Aerodynamics 212 (2021) 104601

Contents lists available at ScienceDirect

Journal of Wind Engineering & Industrial Aerodynamics

journal homepage: www.elsevier.com/locate/jweia

A smart façade system controller for optimized wind-induced vibration mitigation in tall buildings

Khalid M. Abdelaziz [a,*], Alice Alipour [b], Jared D. Hobeck [a]

[a] Alan Levin Dept. of Mechanical and Nuclear Engineering, Kansas State University, Manhattan, KS, USA
[b] Department of Civil, Construction and Environmental Engineering, Iowa State University, Ames, IA, USA

ARTICLE INFO

Keywords:
Wind induced vibration
Smart morphing façade
Tall buildings
Simulation-based optimization
Artificial neural network
Data-driven controllers

ABSTRACT

Wind-induced vibration (WIV) of tall buildings is a major cause of occupant discomfort and potential fatigue damage. Catastrophic failure may also take place at wind speeds that are lower than the design values due to phenomena such as vortex shedding or flutter-induced instabilities. This paper presents a data-driven adaptive control strategy that continuously seeks to minimize WIV for a given average flow condition by independently adjusting the angular orientation of an active façade system composed of a set of plates. The controller utilizes Genetic Algorithm (GA) optimization to determine façade plate angles that minimize time-averaged WIV amplitudes by altering the aerodynamics of the building. The GA is assisted by two artificial neural networks (ANNs). A *predictor* ANN acts as a regression model that continuously estimates the system dynamics. An *optimizer* ANN allows the controller to quickly recall what plate angle combination to use for a given wind condition. A 2D fluid-structure-interaction (FSI) model is used to simulate the steady-state response of the building for given wind conditions and façade plate angle combinations. The 2D model is validated by comparing to published data. Initial results show that vibration amplitudes were reduced up to 94% upon enabling the proposed smart façade controller.

1. Introduction

The number of tall buildings across the world is increasing constantly due to increasing population densities and advancements in building materials, construction technologies and innovative design procedures (Momtaz et al., 2017). A by-product of building taller structures with lighter materials is a reduction in stiffness and damping which makes them more susceptible to unwanted and potentially dangerous wind-induced vibration (WIV) (Momtaz et al., 2017; Poulos 2016; Love et al., 2018).

When the wind attacks a bluff body, such as a building, flow separation on its perimeter causes the formation of vortices of varying velocities and pressure distributions on it surfaces. The distribution of the vortices and their velocity and pressure gradients depend mainly on the geometry of the building as well as the wind conditions (e.g. speed, direction and turbulence intensity) (Hobeck and Inman, 2012, 2014; Sarpkaya, 2004). Even in steady flow conditions, vortex shedding produces fluctuating wind forces that can cause the building to vibrate at frequencies proportional to the wind velocity. When a dominant vortex shedding frequency approaches a natural frequency of the building, a resonance condition can occur resulting in large amplitude vibration (Momtaz et al., 2017). Combined with the low damping capacity of tall buildings, these vibrations adversely affect occupant comfort, cause fatigue damage to building components (Love et al., 2018; Micheli et al., 2018) and may also result in structural or non-structural failures (Sarpkaya 2004; Cao and Sarkar 2013). The development of systems to mitigate wind-induced vibrations has drawn a lot of research interest in recent years because of these concerns (Jafari and Alipour 2021; Micheli et al., 2018).

Different methods have been utilized to combat WIV. These generally include changing the stiffness of the building; adding auxiliary damping devices such as tuned mass damper (TMD) and tuned liquid damper (TLD) systems (Tuan and Shang 2014; Samanta and Banerji 2010; Gardarsson et al., 2001); and aerodynamic modification of the building envelope. Jafari and Alipour have provided an extensive review of these methods (Jafari and Alipour 2021). In general, the mass of both TMD and TLD systems is often high and they often consume space at upper floors of the building where real estate is a precious commodity. Also, TMD and TLD systems are usually tuned for white noise wind excitation disregarding gusts and dominant vortex frequencies (Samanta and Banerji

* Corresponding author.
E-mail address: abdelazizk@ksu.edu (K.M. Abdelaziz).

https://doi.org/10.1016/j.jweia.2021.104601
Received 8 December 2020; Received in revised form 17 February 2021; Accepted 14 March 2021
Available online xxxx

2010). Regarding aerodynamic modification, it is known from various works in the literature that the external geometry and texture of a building has a profound influence on its vortex shedding characteristics (Amini et al., 2018; Hu et al., 2017; Kim and You, 2002; Liu et al., 2021; Sharma et al., 2018; Xie and Yang, 2019). Sharma et al. (2018) concluded that even minor corner modifications to the building (e.g. corner rounding, chamfering) can result in 30–60% reduction in wind-induced loads (Alminhana et al., 2018; Sharma et al., 2018). Major modifications, such as taper and set-back, affect the wind shedding frequencies which reduces the structural response. Sharma et al. also noted that modifications could have adverse effects with different wind flow characteristics and surrounding environments (Lo et al., 2017; Sharma et al., 2018; Yan and Li, 2016).

Adaptive or kinetic building envelopes are currently utilized for shading and energy harvesting as well as for aesthetic purposes (Nagy et al., 2016; Miranda et al., 2020). They are generally composed of louvers, plates or origami modules that can actively alter their orientations or shapes (Nagy et al., 2016; Miranda et al., 2020). Enhancing their functionality by using them as flow-altering mechanisms (as a form of smart aerodynamic shape modifiers), is an innovative approach to help combat WIV in tall buildings. A few studies have addressed such applications in a passive context. Hu et al. (2017) performed wind tunnel tests to study the effect of a double-skin façade. The authors concluded that the double-skin façade with vertical openings can be used to reduce the cross-wind response without inducing a larger along-wind response (Hu et al., 2017). Amini et al. (2018) studied and identified flow controlling blade designs that considerably reduce drag on a smart sustainable housing configuration (Amini et al., 2018). Xie and Yang (2019) presented a case study of a 270 m-high building with plate fairings attached to its corners at a fixed orientation of 45° (Xie and Yang 2019). The authors reported an 18% reduction on structural design wind loads as a result. Yang et al. (2020) analyzed multiple wind tunnel models of buildings having 8 different configurations of vertical plates. The authors reported as much as 50% decrease in the drag force coefficient (Yang et al., 2020). While these studies identify minor corner configurations as an effective means of reducing WIV in tall buildings, the consensus is that an active façade system - rather than a fixed system – would enable it to adapt to changing wind conditions and surrounding environments (Li et al., 2020).

This paper presents a novel smart building façade system designed to actively alter the external geometry of a building in order to obtain aerodynamics that are less susceptible to WIV. The main expected mechanism of operation is the shifting of the dominant wind force frequencies away from the building's natural frequencies. By allowing the façade module orientations to actively change, the system can perform a different aerodynamic modification that suits each wind condition it encounters. When compared to passive aerodynamic modifications, the proposed smart façade system is able to further reduce vibration for any feasible flow condition due to its adaptability. The benefits of the proposed system include: lower cost, less weight, greater aesthetics, adaptability, increased floor space/value, ease of installation, and multifunctionality. As will be shown, only a subset of the plates needs to be controlled, which can allow the remaining ones to serve other purposes of the façade, such as energy saving or energy harvesting.

As an initial study, this work considers only the steady-state behavior of building vibrations. To achieve the aforementioned function in steady-state conditions, a controller needs to be able to (1) measure the free stream wind conditions, (2) measure the current angle orientations for the façade plates, (3) know, in advance, the relationship between (1) and (2) and the resulting steady-state building vibration amplitudes and (4) choose a plate angle combination that minimizes these amplitudes. Items 1 and 2 can be easily performed using a combination of wind velocity sensors (e.g. hot-wire and vane anemometers) and plate motor encoders, respectively. Item 3 is performed in this initial study using fluid-structure-interaction (FSI) simulations that estimate the steady-state building vibration amplitudes resulting from a specific wind condition. It is expected that in an experimental setting or a field deployment, pressure, velocity, and motion sensors would provide this information for the purpose of training the controller. Finally, item 4 is performed using a genetic algorithm (GA) optimization assisted by two artificial neural networks ANNs that dispatches the FSI simulation for different plate angle combinations.

In reality, wind conditions change constantly and sometimes rapidly, which renders a controller that performs a lengthy optimization procedure to make each decision impractical. ANNs, inspired by the human brain, have been shown to successfully perform cognitive tasks that are usually performed by humans such as object, speech and handwriting recognition (Rumelhart and McClelland 1989; Jain et al., 2019; Ptucha et al., 2019). Special ANN designs have also been shown by Kim et al. (2019) to predict the behavior of nonlinear hysteretic systems including the structural response to wind and earthquakes (Micheli et al., 2020; Kim et al., 2019). In the current study, a predictor ANN is utilized as a meta-model to predict the relationship between the flow conditions, plate angles, and the resulting vibration amplitudes. The second ANN is an optimizer which serves as a lookup table that the controller can use directly instead of having to perform a plate angle optimization every time the wind conditions change. To achieve acceptable initial performance, the predictor ANN is trained using FSI simulations (with a potential to use scaled experiments or field observations) and the optimizer ANN is trained using GA optimizations before deployment. The structural characteristics of a building can change over its lifetime, e.g., when bolted joints start to exhibit relaxation (Poulos 2016). The erection of new buildings in the surrounding area may also change the wind turbulence characteristics and the resulting flow-induced forces acting on the building, effectively altering the wind-building system behavior (Lo et al., 2017; Yan and Li, 2016). As will be shown, the control scheme is designed to simultaneously query and train the ANNs, which effectively allows the system to continuously adapt to such changes. The proposed smart façade system is shown to considerably reduce WIV amplitudes by shifting the dominant wind force frequencies away from the building's natural frequencies.

Section 2 of this paper discusses the FSI simulation model and its validation and how it was used to train the ANN algorithm. Section 3 justifies and illustrates the optimization procedure that aims at minimizing the building vibration amplitudes. Section 4 discusses the design of the ANN-based controller and presents a controller simulation case study. Lastly, Section 5 offers a summary of the conclusions and future development for this research.

2. Simulation approach

This section illustrates the simulation approach originally developed by Abdelaziz and Hobeck (2019) (Abdelaziz and Hobeck 2019). The reader may refer to this previous work for details. In addition, the original model is validated herein using experimental data published in the literature for the Commonwealth Advisory Aeronautical Research Council (CAARC) standard building model (Tang and Kwok 2004).

2.1. Fluid model

For the wind speeds considered (less than 10 m/s), air can be assumed to be incompressible (Antonini et al., 2019). Since this study relies on a GA optimization which involves a large number of simulations (~490, see Section 3.3), the Reynolds averaged Navier-Stokes (RANS) equations were utilized because of their low computational cost relative to other methods such as Large Eddy Simulations (LES) (Antonini et al., 2019). Antonini et al. showed that by using wind direction averaging, the RANS k-ω Shear Stress Transport (SST) turbulence model provides accurate predictions for wind speed in the wake of wind turbines (Antonini et al., 2019; Holzmann, 2019). This motivated the adoption of the RANS k-ω SST model in the current study, which performs a considerable amount of building response time averaging while employing separate simulations

for different conditions (see Section 3.3). The equations are discretized using appropriate schemes for each term on a 2D finite volume mesh created using SALOME® (Ribes and Caremoli 2007). The OpenFOAM® (Weller et al., 1998) implementation of the hybrid PIMPLE (PISO + SIMPLE) algorithm is used for time integration as well as pressure-velocity coupling with a dynamic time step that changes to satisfy the Courant-Friedrichs-Lewy (CFL) condition. The condition generally guarantees the time step, the flow velocity and the mesh size are all appropriately proportioned (Holzmann, 2019; Courant et al., 1928). A maximum CFL number of 3 was used, because some of the simulation time steps failed to resolve at higher values, which could negatively affect the validity of the solutions. ParaView software was used throughout this work to visualize and analyze the results (Ayachit 2015).

2.2. Rigid body model

From a design perspective, the in-plane deformations of a floor are negligible when compared with the bending and twisting deformations along the building's height. As a cantilevered structure, the largest vibration amplitudes of the lowest frequency modes generally occur at the free end. Therefore, the simulation in this study considers the top building floor as a 2D, 3-degree of freedom (DOF) rigid body (see Fig. 1). The along- and cross-wind movements of the floor correspond to the bending of the building in two directions, while its rotation corresponds to the torsion in the building. This simplified model cannot account for excitation of the building's higher frequency modes, which would require more than one floor to be simulated and coupled together. It will later be shown in Sections 2.5 and 3.2 that the dominant wind force frequency is either found to be or chosen to be around the lowest natural bending frequency. This minimizes the effects of higher vibration modes, thus justifying the use of the proposed simplified model.

After the pressure and the velocity fields are obtained from the fluid solution, the building height is used along the perimeter to estimate the wind forces. The forces acting on the building and the plates are summed at the geometric center of the floor.

The dynamic response of the top floor as a rigid body with the 3 DOFs explained above is given by the following equation:

$$M\ddot{X} + C\dot{X} + KX = F(t)$$
$$X = [x \quad y \quad \theta]^T \tag{1}$$

where x, y and θ are the along-wind bending, cross-wind bending, and rotational displacements of the floor, respectively. M is the mass matrix, C is the damping matrix, K is the stiffness matrix, $\dot{X}$ is the velocity, $\ddot{X}$ is the acceleration and F is the time varying vector of forces extracted from the CFD simulation at each time step. Equation (1) is solved using the Householder algorithm for symmetric matrices (Householder 1958) to provide the instantaneous values of the accelerations $\ddot{X}$ which are integrated using the simulation time step to obtain $\dot{X}$ and X (Abdelaziz and Hobeck 2019). The coupling between the three DOFs is assumed to be negligible which results in diagonal K, M and C matrices. For the cases being considered, the natural frequency ω for each DOF is known a priori from the literature. System mass and stiffness values were determined by assuming or estimating the stiffness, k, for each DOF, then calculating the mass m with the relationship: $\omega = \sqrt{(k/m)}$. The damping component, c, for each DOF is calculated assuming a damping ratio of 1% which is an acceptable estimate for buildings (Love et al., 2018).

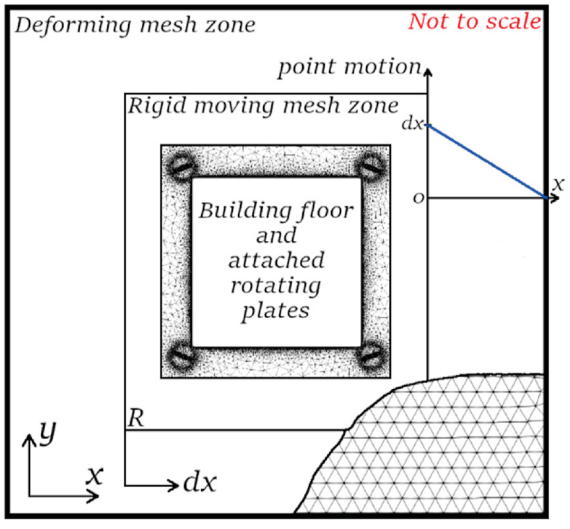

Fig. 1. Motion of mesh points relative to the displacement of the moving region (R).

2.3. Fluid-structure-interaction

After the instantaneous deflections, X, are obtained from the rigid body model, the floor is moved in the CFD mesh accordingly. In reference to Fig. 1, a rectangular region R of the mesh surrounding the building and the plates is assumed to have a constant shape so each point of it is moved according to X. The region R typically extends for about 5 times the building width so that the smallest cells in the mesh (adjacent to the solid body) will not endure any volume changes. The outermost mesh surrounding the region R is the only part of the mesh that is allowed to deform. Its cells expand and contract up to the fixed boundary to accommodate translation and rotation of the building. The motion of each node in this deforming mesh region is determined using linear interpolation between nodes on the boundary of R (full motion) and nodes on the outermost boundary of the computational domain (zero motion). Using linear interpolation allows the mesh to deform gradually to reduce chances of mesh distortion. All mesh point motions are performed by utilizing the OpenFOAM dynamic mesh library (Jasak 2009) which adjusts the mass flow through the cell faces automatically, effectively imposing position and velocity boundary conditions on the fluid domain for the next time step, as per the widely-used partitioned FSI scheme (Banks et al., 2018).

2.4. Four-plate CAARC building

Fig. 2 illustrates the components, dimensions, and coordinate system of the CAARC standard building case. This case is used later in the next

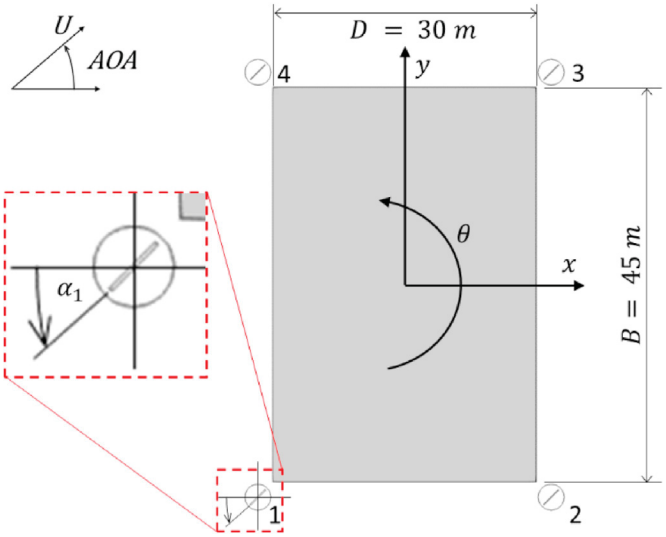

Fig. 2. Layout of the CAARC building floor model with 4 plates at the corners.

section to validate the FSI simulation model. The dimensions of the CAARC building are 180 × 45 × 30 m (Height H× Width B× Depth D); however, a 1:400 scale of these dimensions was used for this study to accommodate future experimental work and to make direct comparisons with results in the literature. A simplified façade consists of four rigid plates which are fixed at the corners of the floor such that they move with it when deflections occur. The plates are placed at corner locations to maximize their potential for altering vortex formation, noting that separation of the incoming flow takes place at the corners. The plate length is approximately 10% of the building width, which is an acceptable ratio for real-life deployment. The plates are assumed to be rigid because the effect of their localized deformations on the building-scale vortex formations is expected to be much smaller than the effect of their angular positions. Additionally, the plate material can be chosen to make them virtually rigid given their small length. In the CFD mesh, each plate is centered inside of a circular mesh boundary which has an interpolation interface with the surrounding mesh. This allows the plates and this circular mesh to rotate freely without requiring re-meshing. The references for measuring angle of attack (AOA) and plate rotation angles are shown in Fig. 2. Table 1 summarizes the final numerical parameters used for the CAARC model.

2.5. Validation

Validation of the proposed FSI model was performed by comparing its displacement power spectral density (PSD) to experimental data from the literature. A PSD can show the structural response, natural frequencies, and dominant vortex shedding response – all of which were used for model validation. Tang et al. (2004) studied the interference effect between adjacent buildings using wind tunnel experiments (Tang and Kwok 2004). Their study includes results for a standard CAARC building as shown in Fig. 2 (without the plates) with no other buildings surrounding it, which was used herein to validate the previously described FSI simulations. Tang also presented vertical wind velocity and turbulence intensity profiles with maximum values of 8.3 m/s and 9%, respectively, measured at the top of the building. This velocity corresponds to approximately 54 m/s for the full-scale building. The natural frequencies for the along-wind bending, cross-wind bending and twisting motions were extracted from the normalized PSD charts provided by Tang et al. (Tang and Kwok 2004). The wind conditions at the top floor were used as inputs to the CFD simulation. Because the proposed model is a 2D representation of a 3D building, it is not able to account for changes in flow conditions along the building height. It is worth mentioning that for this initial model, it is assumed that considering 3D flow effects is not required to demonstrate the smart façade concept and its controller development. In future studies, the authors are planning to account for such effects. The final parameters considered by the simulation are summarized in Table 1.

Table 1
Parameters of the scaled 4-plate two-dimensional CAARC building simulation model.

Parameter	Value	Unit
Along-wind frequency ω_x	12.3	Hz
Cross-wind frequency ω_y	12.8	Hz
Rotational frequency ω_r	18.1	Hz
Damping ratios ζ_x, ζ_y, ζ_r	1%	–
Wind speed U	8.3	m/s
Turbulence intensity I_u	9%	–
Angle of attack AOA	0°	–
Reynolds number RE	60,000	–
Depth D	0.075	m
Width B	0.1125	m
Height H	0.375	m
CFD domain width	3	m
CFD domain height	3	m
Plate width	6×10^{-3}	m
Plate thickness	2.5×10^{-4}	m
Cell count	241,143	

Tang et al. utilized a normalization in their PSD charts that is used in the current study to enable a fair comparison of results (Tang and Kwok 2004). This normalization is given by the following equation:

$$S_{y_n}(n) = \frac{nS_y(n)}{\left[\frac{1}{2k_{y_r}}\rho U^2 BH^2\right]^2} \tag{2}$$

where $S_{y_n}(n)$ is the normalized cross-wind deflection PSD, n is the first mode cross-wind natural frequency of the building, $S_y(n)$ is the cross-wind deflection PSD, ρ is the density of air, k_{y_r} is the rotational stiffness, which equals the applied moment around the base of the building that causes a unit displacement at the top. This stiffness was calculated by multiplying the assumed linear stiffness by the building height. The normalized PSD (Equation (2)) obtained from the wind tunnel experiment performed by Tang et al. and the simulation performed in the current study are plotted versus the reduced frequency ($n_r = nB/U$) in Fig. 3 (Tang and Kwok 2004). The peak wind force frequency obtained from the experiment is only 4% higher than the simulation, which constitutes an acceptable amount of error for this study. The relative differences between the amplitude levels at different frequencies are also in very good agreement. However, the overall amplitude resulting from the simulation developed in this work is higher than the wind-tunnel experiment. This discrepancy exists because the simulation considers only the wind speed at the top of the building (maximum value), and projects this effect along the total height of the building. This results in higher oscillation amplitudes relative to the experiment, which measures the response of a wind velocity profile that shows a reduction in wind speed until it reaches 0 m/s at the ground level (power law). Another potential source of error is the unrealistic turbulence modeling in two-dimensional domains, which eliminates all chaotic fluid motions in the depth dimension. Minor differences in the frequency values may be the result of the digitization process of the plots provided by Tang et al. (Tang and Kwok 2004). Finally, the current study is comparative in nature, which makes the model results useable even if minor numeric differences exist.

3. Amplitude minimization

This section discusses the combined effects of wind conditions and

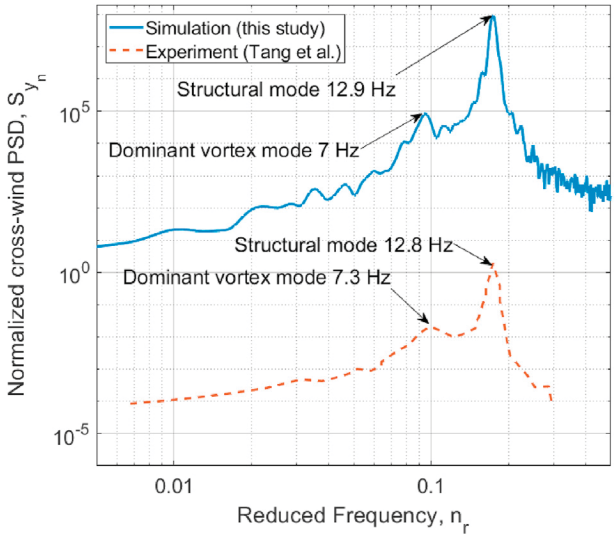

Fig. 3. Comparison between the normalized cross-wind displacement PSDs generated by the proposed two-dimensional simulation (this study) and by experimental data from (Tang and Kwok 2004).

plate angles on building vibration amplitude using the 2D CAARC simulation model illustrated in Section 2.4. The section also discusses a GA amplitude minimization study with a square building geometry having a similar façade plate layout.

3.1. Wind speed and plate angle effect

This section focuses on the 2D four-plate CAARC building model (see Section 2.4) to investigate the relationship between wind speed, plate angles, and building vibration in order to support the feasibility of the proposed smart facades system. Data taken in the United States shows that the average wind speed at 30 m above sea level is in the range of 5–9 m/s, which corresponds to 0.8–1.4 m/s for the 1:400 scale CAARC model used in this study (Pryor et al., 2009). If the plate angle changes are proven to be effective at such low speeds, they will likely be equally or more effective at higher wind speeds. The forces on the building and plates increase with increased wind speed; therefore, control authority and excitation scale together as a function of wind speed.

Fig. 4 compares the simulated power spectral density (PSD) of cross-wind forces on the CAARC building floor at 0.8 and at 1.4 m/s. It can be observed that the peak frequency was shifted from 0.2 to 0.6 Hz as a result of the wind speed change without any changes in the floor geometry or the plate angles. The Strouhal Number, S_t, is used to define the well-known linear relationship between flow velocity, U_H, and vortex shedding frequency, f_s as (Okajima 1982):

$$U_H = \frac{f_s L}{S_t} \tag{3}$$

where L is the characteristic length of a rectangular cylinder. The proposed smart facade system allows this relationship to be controlled rather than being a fixed function with no controllable terms. Fig. 4 also shows the PSD of cross-wind forces at a wind speed of 0.8 m/s when all plate angles are set to 0° (i.e. neutral) and when they are set to 45°. The peak frequencies at 0.19 and 7 Hz were shifted to 0.33 and 9.5 Hz, respectively. This effect was obtained without changing the wind speed. Fig. 5 compares the streamlines of the vortex streets that are formed behind the building for plate orientations of 0° and 45° with an inlet velocity of 0.8 m/s (the same conditions used in Fig. 4). It is clear that the distance between vortex centers decreases when the plates are positioned at 45°. This decrease indicates an increase in vortex shedding frequency as confirmed by the resulting force PSD in Fig. 4. The ratio of the average distance between vortex centers (~1.7) is equal to the shift in the maximum peak frequency (0.33/0.19 ≅ 1.7). These preliminary simulations were performed to explore the effects that drastic changes in plate angles could have on the flow-induced forces. Unlike wind speed and direction, however, the plate orientations are controllable in the framework of the proposed system. These initial results were focused on vortex shedding forces of an isolated building, but it is important to recognize that wind-induced excitation on buildings is caused by a combination of vortex shedding, buffeting, and upstream turbulence. Therefore, a more exhaustive study seeking to minimize building vibration was performed for independent plate orientations.

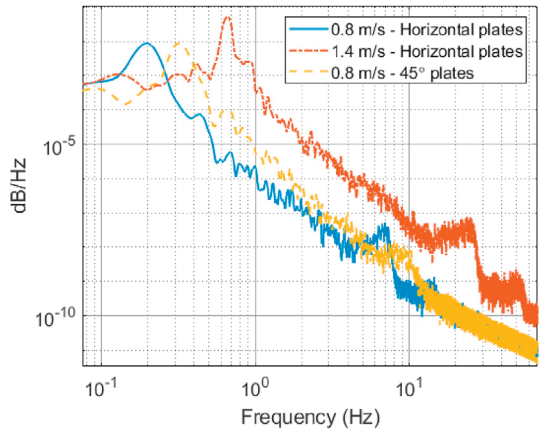

Fig. 4. PSD of cross-wind forces obtained from simulation of the CAARC scaled model.

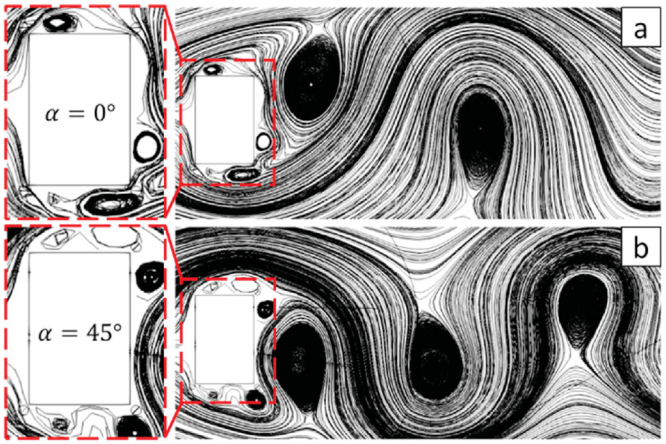

Fig. 5. Vortex street formed behind the building at 0.8 m/s wind speed for (a) horizontal plates and (b) plates tilted 45.°

3.2. Optimization case

The CAARC building case was used in previous sections to validate the simplified model, meshing, and simulation parameters because there is published experimental data readily available in the literature (Tang and Kwok 2004). The focus then shifted toward quantifying the relationship between plate angles, flow velocity, and building vibration. Because the goal of this study is to minimize vibration by controlling the plate angles, an optimization was performed based on an arbitrary 1 m square building floor as shown in Fig. 2. Except for the floor geometry being square rather than rectangular, the overall dimensions and plate locations of the optimization case are similar to those of the four-plate CAARC building case (see Fig. 2) with a scale of approximately 1:40. A square geometry was used to produce symmetry and reduce the wind AOA values that need to be considered. It was decided to use an inlet wind speed U_H that would cause the vortex shedding frequency f_s of the building with no plates to be approximately equal to the building's bending natural frequency (f=0.6 Hz). At the simulation Reynolds number Re of 300,000, the Strouhal number is approximately equal to 0.13 (Okajima 1982). As expected, this near-resonance condition ($f \approx f_s$) produced the largest vibration amplitudes and was considered a worst-case flow speed scenario that would help demonstrate the effectiveness of the smart facade system. If, for example, another velocity was arbitrarily chosen and produced a vortex shedding frequency far from the natural frequency, then the resulting vibration would be significantly smaller, and a plate angle optimization would produce only marginal improvements. Table 2 summarizes the final optimization case simulation parameters.

3.3. Genetic algorithm

The proposed optimization problem aims to find the plate angle combination that minimizes steady-state building deflection amplitude. The objective function was formulated as follows:

$$max.\, f(\alpha_i) = \frac{0.1}{\sqrt{\sigma_x^2 + \sigma_y^2 + 10^8 \sigma_\theta^2}} \; for \begin{cases} 0 \le \alpha_i \le \pi \\ i = 1, 2, 3, 4 \end{cases} \tag{4}$$

Table 2
Parameters of the 1 m square building optimization case.

Parameter	Value	Unit
Along-wind frequency ω_x	0.6	Hz
Cross-wind frequency ω_y	0.6	Hz
Rotational frequency ω_r	41.7	Hz
Damping ratios ζ_x, ζ_y, ζ_r	1%	–
Wind speed U	5.0	m/s
Turbulence intensity I_u	9%	–
Angle of attack *AOA*	0°	–
Reynolds Number RE	3×10^5	
Depth D	1	m
Width B	1	m
Height H	3.3	m
CFD domain width	21	m
CFD domain height	21	m
Plate width	0.1	m
Plate thickness	2.5×10^{-3}	m
Cell count	62,800	

where σ^2 is the 30-s statistical variance of building floor oscillations for all DOFs, which represents the deflection amplitude, and α_i is the rotation angle of plate i as illustrated in Fig. 2. Because the building deflection angle is small and measured in radians, its variance σ_θ^2 is multiplied by 10^8 to make all three variances equally significant. Evaluating Equation (4) requires an FSI simulation similar to that discussed in Section 2. The simulation runs until the sum of variance (Equation (4)) stays within a prespecified tolerance, thus indicating that the system has settled into a steady-state time-averaged response. This running 30-s deflection variance (similar to a running average) was used to quantify the time-averaged deflection amplitudes during simulation rather than the instantaneous deflection amplitudes. Though the instantaneous forces acting on the building have higher inaccuracies with the RANS k-ω SST turbulence model for high flow separation cases, Antonini et al. (2019) showed that averaging the resulting structural response minimizes these inaccuracies thus making the RANS model a more efficient valid option for predicting the time-averaged structural response (Antonini et al., 2019). To start the optimization, the objective function was evaluated for different randomly chosen plate angle combinations. The relationship was not found to be monotonic, which means that multiple local optima may exist. Therefore, a global optimization technique, such as GAs, was used instead of a direct search method to avoid convergence to local optimum solutions. A GA program was written in C++ that operates one generation at a time using an input/output "generation" file (comma--separated list). If there was no previous generation file provided, the GA program begins by generating a uniformly random population of 70 different plate angle combinations and writes them down to a newly created generation file. An independent simulation is performed for each plate angle combination, and the objective function (Equation (4)) is evaluated and inserted into the same text file. The GA code reads the file again to determine the angles to be evaluated in the next generation. The 10 best performing plate angle combinations are copied to the next generation as elites. Fitness-proportionate selection (roulette wheel) is used to determine the remaining 60 combinations to be evaluated. Single-point cross over is performed with a probability of 0.8 as well as uniform mutation with a probability of 0.1. A new file is written for the new generation and the process is repeated until the GA stops finding better combinations. The population size and the mutation and cross-over rates were determined from recommendations in the literature (Angelova and Pencheva 2011). The developed GA was also tested against a number of benchmark problems to ensure proper implementation (Jamil and Yang 2013).

The optimization was run for a total of 7 generations, which involved performing approximately $7 \times 70 = 490$ simulations, each of which considers a different 4-plate rotation angle combination. It is expected that the interaction between the different values of plate rotation angles α_i will have a significant effect on the overall building response. The GA optimization and the control algorithm (see Section 4) account for these complex aeroelastic interactions indirectly by observing the time-averaged building response (Equation (4)). The GA uses uniform cross-over to recombine plate angle combinations where fitness proportionate selection makes it more likely to consider plate angle combinations that will reduce building vibration. Each simulation in the optimization utilizes 12 processor cores from the CRUNCH computational cluster at the Multifunctional Structures Laboratory (MSL) at Kansas State University, which allows up to 24 plate angle combinations to be simulated simultaneously. Fig. 6 shows the GA convergence for 7 generations as well as the corresponding optimum plate combinations. The average fitness is shown to steadily increase from a generation to the next, which indicates the effectiveness of the optimization procedure. However, only two performance improvements were obtained relative to the initial generation. This suggests that running more generations may obtain better solutions, but the corresponding improvements are expected to be minimal compared to the additional computational effort. Further optimization is planned to be performed in a future study using an experimental setup, to validate this optimization approach with online learning and optimization.

3.4. Optimization results

Fig. 7 compares the time series for along-wind, cross-wind and torsional building oscillations, respectively, between the optimal and a suboptimal solution. The *suboptimal* solution is the average performance from the first GA generation (i.e. whose fitness approximately equals the average fitness in generation 1). The simulated steady state amplitudes of building oscillations show a decrease of 60–80%. It is important to note that these simulation results may not quantitatively relate to a full-scale deployed system; however, they do indicate that the controller is able to operate as expected. This reduction can be explained in light of the PSD plot in Fig. 8 where the optimum configuration decreases the force amplitude around the bending mode natural frequency of 0.6 Hz. This causes a more significant proportion of the available wind energy to avoid frequencies most sensitive to the building, which results in a lower amplitude response around that frequency as evident in the deflection PSD. As shown in the force PSD, the peak at the natural frequency (0.6 Hz) is not very prominent, which means that multiple phenomena may have been involved (e.g. turbulent buffeting). However, this minimal representation of the smart façade system (only 4 plates) still

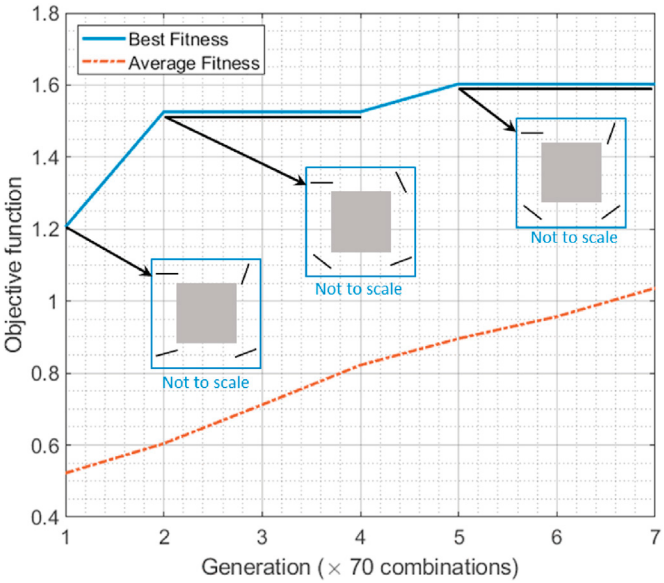

Fig. 6. Convergence trends for the genetic algorithm optimization process showing the optimum plate configurations for different generations.

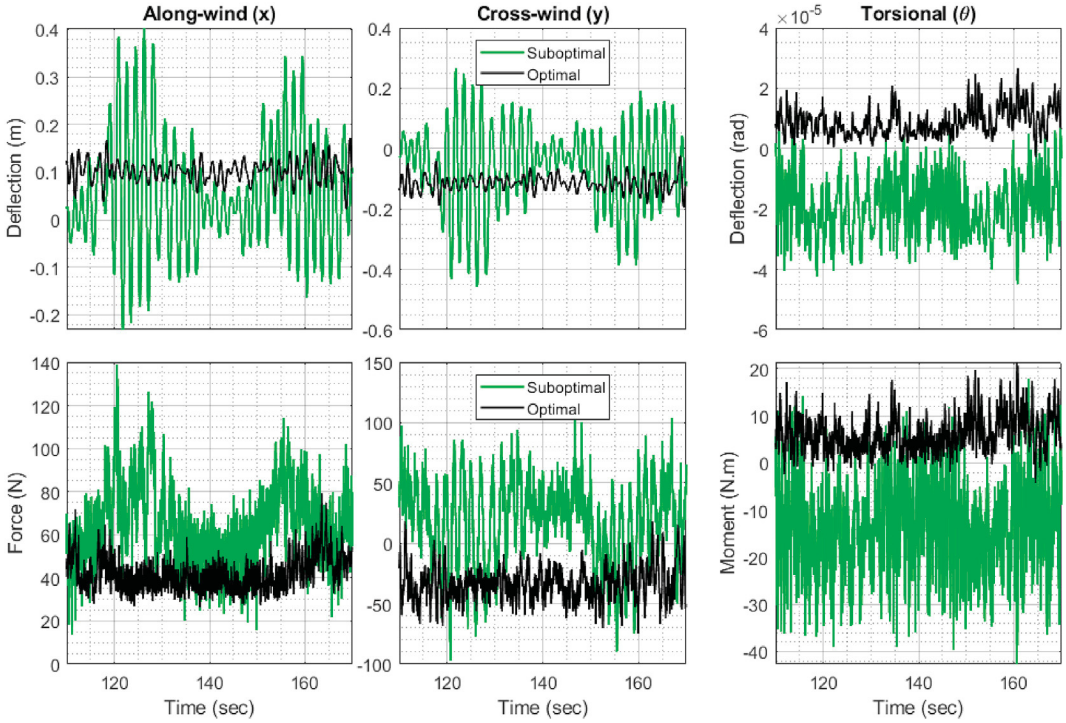

Fig. 7. Comparison between the suboptimal and the optimal deflections and forces for all 3 DOFs.

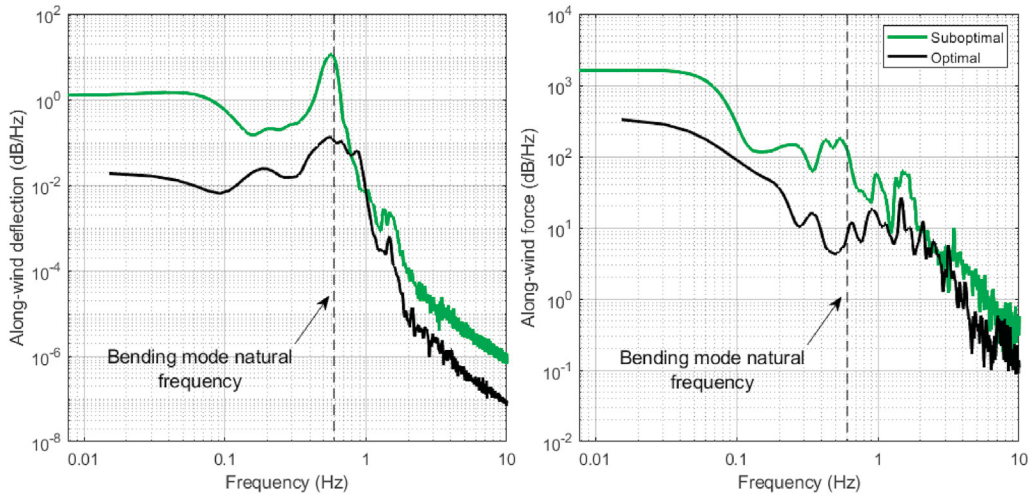

Fig. 8. Comparison of the along-wind building deflection and wind force PSDs before and after plate angle optimization.

considerably reduced building oscillations, which is a good indicator of robustness and prompts related ongoing and future work.

4. Controller design

The proposed controller operates by treating the plate-wind-building system as a reduced order system controlled only by knowing the inputs (plate orientation angles α_i, average windspeed and angle of attack) and the outputs (building deflections). This allows the controller to operate efficiently without requiring knowledge of the complex turbulent flow surrounding the plates and the building. It is understood that the position of a single plate has the potential to influence the flow around a nearby or downstream plate; however, instead of trying to observe and quantify those interactions the controller operates on parameters that are more practical to measure (e.g., building motion) using existing sensing techniques. Two ANNs are utilized by the controller to issue plate angle control actions. A predictor ANN acts as a regression model that provides estimates of the system dynamics, represented by the variance sum described in Section 3.3. An optimizer ANN is used directly by the controller to decide on the plate angles to use for a given wind condition. Fig. 9 shows the layout of the designed ANN-based controller. The predictor ANN is shown to have the wind condition and the plate angles as input, both of which are expected to significantly affect the variance sum as illustrated in Section 3.2. For simplicity, the wind condition is represented only by the wind speed in this study. However, including the AOA and turbulence measurements as inputs is a possible extension. Sufficient averaging of wind condition readings can be performed to reduce plate actuation speed requirements. After the controller issues plate angle commands using the optimizer ANN, the deflection variances are measured using accelerometers mounted on the building. The controller

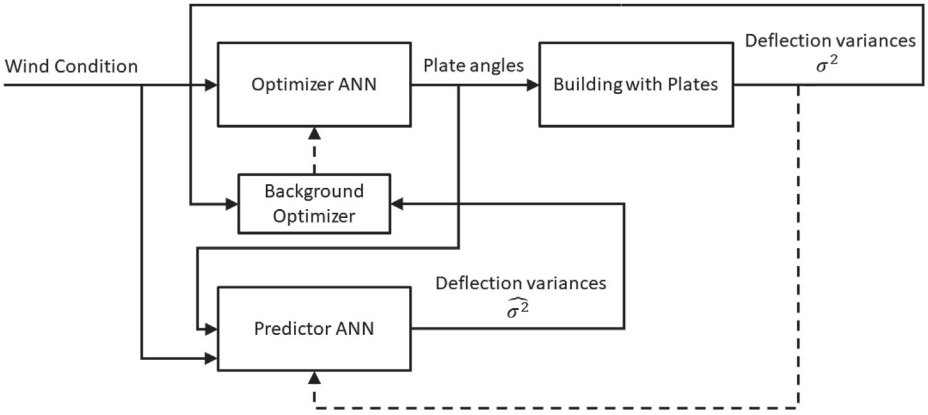

Fig. 9. ANN-based controller operation schematic (dashed lines indicate learning paths).

keeps track of the deflection variances that result at different plate angle combinations and wind conditions so they can be used to periodically train the predictor ANN. The background optimizer is a GA optimizer which uses the predictor ANN as a meta model. It constantly tries to find better plate angle combinations for the wind conditions being encountered by the controller. The findings of the background optimizer are also used to periodically train the optimizer ANN when a better solution is found.

4.1. Predictor ANN

An ANN-based meta-model for estimating the deflection amplitudes (variances) is used because: (1) it can generalize from conditions of simulated behavior to conditions of unknown behavior; and (2) it can be used in real-time, because its evaluation is computationally inexpensive, when compared with simulation. Various ANN architectures and configurations were considered with the goal of obtaining an accurate regression. The final architecture has two hidden layers, each consists of 10 neurons which use the bipolar sigmoid activation function. This function was used because it is expected to be able to correctly map nonlinear behavior as well as positive and negative values. The ANN was trained using ~500 different wind speed and plate combinations. Only 70% of this total was used to train the network using backpropagation learning. The learning was performed for minibatches of 16 data points. Stochastic gradient descent (SGD) was used as an optimization algorithm (Amari 1993). The learning rate, which controls the amount of change in the network weights per update, was set at 0.001. The remaining 30% of the data was used only in the final testing stage to evaluate the Root mean square error (RMSE) for the prediction. Fig. 10 illustrates the performance of the predictor ANN for the range of plate angles simulated. An RMSE of 1 mm for the variance sum was obtained, which is equal to an acceptable value of 40 mm for the full-scale building. Additionally, for a deployed system, as per the controller design (see Fig. 9), the predictor ANN has a learning path (indicated by a dashed line in the figure) which compares deflection variances σ^2 calculated from online sensor measurements, to the current estimation of deflection variances $\widehat{\sigma^2}$ and updates network weights accordingly. The sensors utilized for this purpose could simply be building-mounted accelerometers whose output can be integrated to obtain the deflection variances (Vaccaro et al., 2006). This learning process can be performed indefinitely, which is expected to continuously improve the prediction accuracy and enable the predictor ANN to adjust to long term environmental or building changes.

4.2. Optimizer ANN

It is possible for the controller to use the predictor ANN illustrated in the previous section as a meta-model to issue plate angle change

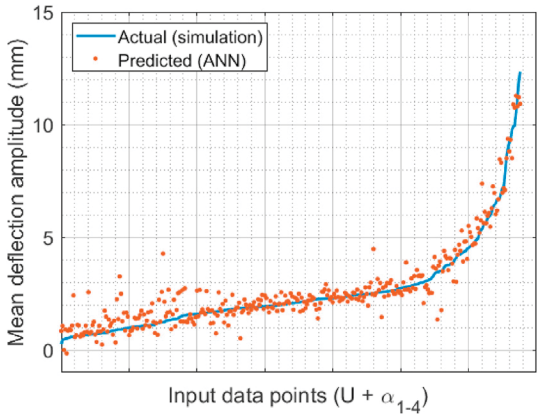

Fig. 10. Result of predictor ANN training showing actual and predicted deflection amplitudes for various combinations of wind velocity and plate angles.

commands, but it would require performing a minimum-amplitude optimization for each control step. The delay incurred due to these searches is impractical for real-time actuation and would render the controller useless. Instead, the optimizer ANN serves as a direct lookup for the controller. For a given wind condition it instantly provides the optimum plate angle combination. The background optimizer illustrated in Fig. 9 trains the optimizer ANN by evaluating what-if scenarios in an off-line manner. This allows training to be disconnected from the main controller loop and be performed selectively with regard to available computational resources and the need for a better solution. The training utilizes a GA optimization, similar to Section 3.3, but uses the predictor ANN as a meta-model instead of using FSI simulations. When this background optimization finds an optimum plate angle combination for a specific wind condition, the difference between the current optimum and the new optimum is used to train the optimizer ANN by updating its connection weights. Because both ANNs can be trained indefinitely, the controller as a whole can adapt to changes in the building or environment. Evaluating performance of the optimizer ANN using FSI simulations is a very time-consuming process, because the optimization in Section 3.3 would need to be restarted for each new wind condition. It was decided to perform this more exhaustive adaptive control evaluation via experiment in a future study because online learning can occur in real-time orders of magnitude faster than would be possible with simulation.

4.3. Controller simulation

The optimization case illustrated in Section 3.2 was also used to

perform a simulation of the controller performance. The purpose is to evaluate the amount of time it takes the plate angle changes to affect the vortex system and obtain a tangible difference in the building oscillations. Fig. 11 shows the along-wind time response of the building to the following simulation procedure: The wind speed at the inlet is set at 5 m/s, similar to the original case. The plates are set at a suboptimal configuration and the fluid domain is left to stabilize while the building deflection is held constant. After the fluid forces develop, the building is allowed to move, which causes building oscillations with approximately 10 mm amplitudes to ensue. When the controller changes plate angles to their optimum configuration for 5 m/s (see Section 3.4), the oscillations diminish to only 0.6 mm in approximately 7 s (94% reduction). A considerable reduction of 60% is obtained after only 3 s. Again, it is important to note that these results may not quantitatively represent real-life deployment performance due to the 2D simplifications made to the model. However, these results do bring validity to the proposed control scheme – the focus of this study – while motivating future work to focus on scaled 3D building experiments.

These results demonstrate that the plates, building, and controller are able to respond fast enough to negate wind events that may last up to 20 s, or at least speed up the decay of the resulting oscillations after the events occur. Wind gusts usually last less than 20 s; however, longer-lasting strong winds which are called squalls can continue for minutes. Tornadoes can last from several seconds to more than an hour, but are typically less than 10 min (U. S. Department of Commerce 2020; American Meteorological Society, 2020). The life cycle of a hurricane can be anywhere from 12 h to a month (Hurricane Science 2020). Thunderstorm winds may last tens of minutes, and local breezes generated by heating of land surfaces can last a few hours.

An important limiting factor is how fast the plates can be rotated to new locations. This can be considered when designing the full system by making the plates light enough to allow for speedy actuation. Reducing plate weight may be accomplished numerous ways including reducing plate height and making them from lightweight material (e.g. composites). Adding more plates (instead of only 4) and reducing their size may also help to improve plate rotation speeds. While these modifications are viable approaches that could be considered in the context of a parametric study to improve the performance of the system, they are outside the scope of this study which focuses on underlining the effectiveness of the control algorithm.

5. Conclusions

The development of a smart façade controller to mitigate wind-induced vibrations in tall buildings was illustrated in this work. Fluid-solid-interaction (FSI) simulations were utilized to verify and illustrate how changing the façade module orientations reduce the building oscillation amplitudes. The simulation methodology was first validated in the frequency domain using published data for a scaled model of the standard Commonwealth Advisory Aeronautical Research Council (CAARC) building and a good agreement was obtained. The response of a CAARC building with 4 controllable plates attached to its corners was investigated at different plate angles and wind speeds. It was found that varying the plate angle shifts the frequency of the vortex-induced forces significantly. A Genetic Algorithm (GA) optimization procedure was implemented to obtain plate angle combinations that minimized building deflection amplitudes. An amplitude reduction of 60–80% was obtained as a result of the optimization. The deflection data collected during the optimization was used to train a predictor-optimizer Artificial Neural Network (ANN) system which was designed to be used by the controller in real-time operation upon deployment. The prediction performance of the ANN system was found to be acceptable with a deflection RMSE of ~1 mm. Additionally, the proposed controller is able to continuously train the ANN system using sensor measurements as well as offline background GA optimizations to keep improving its predictions, without causing controller/actuator delays which would diminish performance. This ANN-based controller provides for adaptation to changes in the environment and in the building. Finally, the controller performance was evaluated using a separate simulation procedure. It was found to be able to reduce the oscillation amplitudes by 60% in 3 s and by 94% in 7 s. The plate rotation speed was identified as an important limiting factor for the developed smart morphing facade system, which means that the plates should be sized and designed to allow for speedy actuation. The findings of this study motivate future work to focus on scaled 3D building experiments to analyze complete system performance with a greater variety of feasible wind conditions.

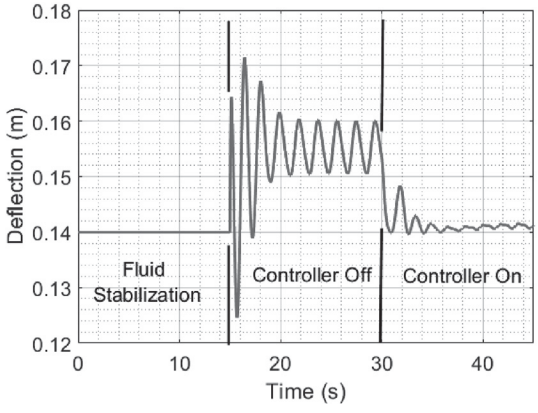

Fig. 11. Along-wind deflection changes as a result of employing the smart façade ANN-based controller.

CRediT authorship contribution statement

Khalid M. Abdelaziz: Methodology, Software, Validation, Formal analysis, Investigation, Writing – original draft, Visualization. **Alice Alipour:** Conceptualization, Resources, Writing – review & editing, Project administration, Funding acquisition. **Jared D. Hobeck:** Conceptualization, Methodology, Software, Resources, Writing – review & editing, Supervision, Project administration, Funding acquisition.

Declaration of competing interest

No known conflicts of interest.

Acknowledgments

This material is based upon work supported by the National Science Foundation, United States under Grant Number CMMI-1826364.

References

Abdelaziz, K.M., Hobeck, J.D., 2019. Developing a smart façade system controller for wind-induced vibration mitigation in tall buildings ASME 2019 conference on smart materials. Adaptive Structures and Intelligent Systems. https://doi.org/10.1115/smasis2019-5674.

Alminhana, G.W., Braun, A.L., Loredo-Souza, A.M., 2018. A numerical-experimental investigation on the aerodynamic performance of CAARC building models with geometric modifications. J. Wind Eng. Ind. Aerod. 180, 34–48. https://doi.org/10.1016/j.jweia.2018.07.001.

Amari, S.-i., 1993. Backpropagation and stochastic gradient descent method. Neurocomputing 5 (4–5), 185–196. https://doi.org/10.1016/0925-2312(93)90006-o.

American Meteorological Society (2020), [Online], Available: www.ametsoc.org.

Amini, K., Mortazavi, S.M., Rezaian, E., Najafi, A.F., 2018. Numerical investigation on the convection heat transfer and drag reduction by utilizing the designed flow controlling blades on a smart sustainable house. Energy Efficiency 12 (3), 757–776. https://doi.org/10.1007/s12053-018-9706-9.

Angelova, M., Pencheva, T., 2011. Tuning genetic algorithm parameters to improve convergence time. International Journal of Chemical Engineering 2011. https://doi.org/10.1155/2011/646917, 1–7.

Antonini, E.G.A., Romero, D.A., Amon, C.H., 2019. Improving CFD wind farm simulations incorporating wind direction uncertainty. Renew. Energy 133, 1011–1023. https://doi.org/10.1016/j.renene.2018.10.084.
Ayachit, U., 2015. The ParaView Guide (Full Color Version): A Parallel Visualization Application. Kitware, Incorporated.
Banks, J.W., Henshaw, W.D., Schwendeman, D.W., Tang, Q., 2018. A stable partitioned FSI algorithm for rigid bodies and incompressible flow in three dimensions. J. Comput. Phys. 373, 455–492. https://doi.org/10.1016/j.jcp.2018.06.072.
Cao, B., Sarkar, P.P., 2013. Time-domain aeroelastic loads and response of flexible bridges in gusty wind: prediction and experimental validation. J. Eng. Mech. 139 (3), 359–366. https://doi.org/10.1061/(asce)em.1943-7889.0000502.
Courant, R., Friedrichs, K., Lewy, H., 1928. Über die partiellen Differenzengleichungen der mathematischen Physik. Math. Ann. 100 (1), 32–74. https://doi.org/10.1007/bf01448839.
Gardarsson, S., Yeh, H., Reed, D., 2001. Behavior of sloped-bottom tuned liquid dampers. J. Eng. Mech. 127 (3), 266–271. https://doi.org/10.1061/(ASCE)0733-9399(2001)127:3(266).
Hobeck, J.D., Inman, D.J., 2012. Artificial piezoelectric grass for energy harvesting from turbulence-induced vibration. Smart Mater. Struct. 21 (10), 105024. https://doi.org/10.1088/0964-1726/21/10/105024.
Hobeck, J.D., Inman, D.J., 2014. A distributed parameter electromechanical and statistical model for energy harvesting from turbulence-induced vibration. Smart Mater. and Struct. 23 (11), 115003. https://doi.org/10.1088/0964-1726/23/11/115003.
Holzmann, T., 2019. Mathematics, Numerics, Derivations and OpenFOAM®, Holzmann CFD, 7th. Holzmann CFD.
Householder, A.S., 1958. Unitary triangularization of a nonsymmetric matrix. J. ACM 5 (4), 339–342. https://doi.org/10.1145/320941.320947.
Hu, G., Hassanli, S., Kwok, K.C.S., Tse, K.T., 2017. Wind-induced responses of a tall building with a double-skin façade system. J. Wind Eng. Ind. Aerod. 168, 91–100. https://doi.org/10.1016/j.jweia.2017.05.008.
Hurricane science, 2020 [Online], Available. www.hurricanescience.org.
Jafari, M., Alipour, A., 2021. Methodologies to mitigate wind-induced vibration of tall buildings: a state-of-the-art review. Journal of Building Engineering 33. https://doi.org/10.1016/j.jobe.2020.101582.
Jain, D.K., Shamsolmoali, P., Sehdev, P., 2019. Extended deep neural network for facial emotion recognition. Pattern Recogn. Lett. 120, 69–74. https://doi.org/10.1016/j.patrec.2019.01.008.
Jamil, M., Yang, X.S., 2013. A literature survey of benchmark functions for global optimisation problems. Int. J. Math. Model. Numer. Optim. 4 (2), 150. https://doi.org/10.1504/ijmmno.2013.055204.
Jasak, H., 2009. Dynamic mesh handling in OpenFOAM 47th. AIAA Aerospace Sciences Meeting including The New Horizons Forum and Aerospace Exposition. https://doi.org/10.2514/6.2009-341.
Kim, T., Kwon, O.-S., Song, J., 2019. Response prediction of nonlinear hysteretic systems by deep neural networks. Neural Network. 111, 1–10. https://doi.org/10.1016/j.neunet.2018.12.005.
Kim, Y.-M., You, K.-P., 2002. Dynamic responses of a tapered tall building to wind loads. J. Wind Eng. Ind. Aerod. 90 (12–15), 1771–1782. https://doi.org/10.1016/s0167-6105(02)00286-6.
Li, Y., Li, C., Li, Q.-S., Song, Q., Huang, X., Li, Y.-G., 2020. Aerodynamic performance of CAARC standard tall building model by various corner chamfers. J. Wind Eng. Ind. Aerod. 104197. https://doi.org/10.1016/j.jweia.2020.104197.
Liu, J., Hui, Y., Yang, Y., Tamura, Y., 2021. Flow field investigation for aerodynamic effects of surface mounted ribs on square-sectioned high-rise buildings. J. Wind Eng. Ind. Aerod. 211, 104551. https://doi.org/10.1016/j.jweia.2021.104551.
Lo, Y.-L., Kim, Y.C., Yoshida, A., 2017. Effects of aerodynamic modification mechanisms on interference from neighboring buildings. J. Wind Eng. Ind. Aerod. 168, 271–287. https://doi.org/10.1016/j.jweia.2017.06.018.
Love, J.S., Haskett, T.C., Morava, B., 2018. Effectiveness of dynamic vibration absorbers implemented in tall buildings. Eng. Struct. 176, 776–784. https://doi.org/10.1016/j.engstruct.2018.09.050.
Micheli, L., Alipour, A., Laflamme, S., 2018. Performance-Based Design for Wind-Excited Tall Buildings Equipped with High Performance Control Systems. https://doi.org/10.1061/9780784481325.019.
Micheli, L., Hong, J., Laflamme, S., Alipour, A., 2020. Surrogate models for high performance control systems in wind-excited tall buildings. Appl. Soft Comput. 90, 106133. https://doi.org/10.1016/j.asoc.2020.106133.
Miranda, R., Babilio, E., Singh, N., Santos, F., Fraternali, F., 2020. Mechanics of smart origami sunscreens with energy harvesting ability. Mech. Res. Commun. 105, 103503. https://doi.org/10.1016/j.mechrescom.2020.103503.
Momtaz, A.A., Abdollahian, M.A., Farshidianfar, A., 2017. Study of wind-induced vibrations in tall buildings with tuned mass dampers taking into account vortices effects. International Journal of Advanced Structural Engineering 9 (4), 385–395. https://doi.org/10.1007/s40091-017-0174-9.
Nagy, Z., Svetozarevic, B., Jayathissa, P., Begle, M., Hofer, J., Lydon, G., Willmann, A., Schlueter, A., 2016. The adaptive solar facade: from concept to prototypes. Frontiers of Architectural Research 5 (2), 143–156. https://doi.org/10.1016/j.foar.2016.03.002.
Okajima, A., 1982. Strouhal numbers of rectangular cylinders. J. Fluid Mech. 123, 379–398. https://doi.org/10.1017/s0022112082003115.
Poulos, H.G., 2016. Tall building foundations: design methods and applications. Innovative Infrastructure Solutions 1 (1), 10. https://doi.org/10.1007/s41062-016-0010-2.
Pryor, S.C., Barthelmie, R.J., Young, D.T., Takle, E.S., Arritt, R.W., Flory, D., Gutowski, W.J., Nunes, A., Roads, J., 2009. Wind speed trends over the contiguous United States. J. Geophys. Res. 114 (D14) https://doi.org/10.1029/2008jd011416.
Ptucha, R., Such, F.P., Pillai, S., Brockler, F., Singh, V., Hutkowski, P., 2019. Intelligent character recognition using fully convolutional neural networks. Pattern Recogn. 88, 604–613. https://doi.org/10.1016/j.patcog.2018.12.017.
Ribes, A., Caremoli, C., 2007. In: Salome Platform Component Model for Numerical Simulation Proceedings of the 31st Annual International Computer Software and Applications Conference, pp. 553–564. https://doi.org/10.1109/COMPSAC.2007.185, 02, Washington.
Rumelhart, D.E., McClelland, J.L., 1989. Parallel Distributed Processing: Explorations in the Microstructure of Cognition. The MIT Press. Available. https://www.amazon.com/Parallel-Distributed-Processing-Explorations-Microstructure/dp/B00BUQ7768?SubscriptionId=AKIAIOBINVZYXZQZ2U3A&tag=chimbori05-20&linkCode=xm2&camp=2025&creative=165953&creativeASIN=B00BUQ7768.
Samanta, A., Banerji, P., 2010. Structural vibration control using modified tuned liquid dampers. IES J. Part A Civ. Struct. Eng. 3 (1), 14–27. https://doi.org/10.1080/19373260903425410.
Sarpkaya, T., 2004. A critical review of the intrinsic nature of vortex-induced vibrations. J. Fluid Struct. 19 (4), 389–447. https://doi.org/10.1016/j.jfluidstructs.2004.02.005.
Sharma, A., Mittal, H., Gairola, A., 2018. Mitigation of wind load on tall buildings through aerodynamic modifications: Review. Journal of Building Engineering 18, 180–194. https://doi.org/10.1016/j.jobe.2018.03.005.
Tang, U.F., Kwok, K.C.S., 2004. Interference excitation mechanisms on a 3DOF aeroelastic CAARC building model. J. Wind Eng. Ind. Aerod. 92 (14–15), 1299–1314. https://doi.org/10.1016/j.jweia.2004.08.004.
Tuan, A.Y., Shang, G.Q., 2014. Vibration control in a 101-storey building using a tuned mass damper. Journal of Applied Science and Engineering 17, 141–156. https://doi.org/10.6180/jase.2014.17.2.05.
U. S. Department of Commerce, 2020. National weather service [Online], Available. http://www.noaa.gov.
Vaccaro, R.J., Gindy, M., Nassif, H., Velde, J., 2006. An algorithm for estimating bridge deflection from accelerometer measurements 2006 fortieth asilomar conference on signals. Systems and Computers. https://doi.org/10.1109/acssc.2006.354806.
Weller, H.G., Tabor, G., Jasak, H., Fureby, C., 1998. A tensorial approach to computational continuum mechanics using object-oriented techniques. Comput. Phys. 12 (6), 620. https://doi.org/10.1063/1.168744.
Xie, J., Yang, X.-y., 2019. Exploratory study on wind-adaptable design for super-tall buildings. Wind Struct. 29 (6), 489–497. https://doi.org/10.12989/was.2019.29.6.489.
Yan, Bowen, Li, Q.-S., 2016. Wind tunnel study of interference effects between twin super-tall buildings with aerodynamic modifications. J. Wind Eng. Ind. Aerod. 156, 129–145. https://doi.org/10.1016/j.jweia.2016.08.001.
Yang, Q., Liu, Z., Hui, Y., Li, Z., 2020. Modification of aerodynamic force characteristics on high-rise buildings with arrangement of vertical plates. J. Wind Eng. Ind. Aerod. 200, 104155. https://doi.org/10.1016/j.jweia.2020.104155.